Preprint of paper which appeared in the Proceedings of the
16th International Conference on Climbing and Walking Robots and the
Support Technologies for Mobile Machines

MODEL-BASED ELASTIC TENDON CONTROL FOR ELECTRICALLY ACTUATED MUSCULOSKELETAL BIPEDS

K. RADKHAH∗ and O. VON STRYK

Department of Computer Science, Technische Universität Darmstadt,
64289 Darmstadt, Germany
∗E-mail: radkhah@sim.tu-darmstadt.de
www.sim.tu-darmstadt.de

Human-inspired musculoskeletal design of bipedal robots offers great potential towards enhanced dynamic and energy-efficient locomotion but imposes also major challenges on their control. In this paper we present an analytical model-based controller that takes into account the system's complex musculoskeletal actuation dynamics in order to fully exploit the intrinsic dynamics. The effectiveness of the proposed approach is evaluated for hopping-in-place motions on the simulation model of the BioBiped1 robot, a human-inspired musculoskeletal biped featuring a highly compliant tendon-driven actuation system.

1. Introduction

This paper addresses the challenging question of motion generation for a musculoskeletal biped with three-segmented legs driven by a number of active and passive, mono- and biarticular structures. Despite recent increase in popularity (see Refs. 1–4), such designs are so far quite unique and open up a number of questions regarding the degree of design complexity and suitable control concepts. For pneumatically actuated systems basic feedforward controllers for the operation of the valves have been employed based on ground contact sensing to realize walking, running and jumping motions.[5] The timely operation of the valves based on experimental tuning was particularly important since the structures can get in the way of each other. Sinusoidal excitation of electrical motors may be successful for rather simple mechanical systems with few passive parameters and with linear or even direct drive transmissions.[6] An important issue to be considered during a such motion generation process is choosing the step frequency

correctly, which is quite difficult for a nonlinear complex musculoskeletal leg design. Second, not all motions can be represented by basic sinusoids. Further, particularly in case of nonlinear actuation dynamics, identifying the corresponding motor actions without model knowledge is not feasible.

Therefore, for these kind of complex musculoskeletal systems we suggest a model-based approach for trajectory planning and execution. Using a similar concept, introduced in Ref. 7 for flexible manipulators, an earlier version of this method had been successfully applied to a bipedal robot with a very basic linear elastic actuation system for dimensioning the required motor-gearboxes.[8] In this paper we describe and discuss the approach in a detailed manner exemplary for the complex nonlinear elastic actuation system of the bipedal robot BioBiped1, a novel highly elastic actuation system comprising human-inspired active and passive mono- and biarticular muscle-tendon structures.[9] As proof of concept, the method is applied in simulation to the identified robot model to generate hopping-in-place motions. The resulting motions are compared to motions obtained by motor excitation, a quite popular approach often employed for underactuated robots. It is demonstrated that the model-based approach is capable of realizing the desired motions without increasing the power consumption. Furthermore, comparability and evaluation of different leg actuation designs for diverse gaits and performance criteria are facilitated by this method.

2. BioBiped's Musculoskeletal Actuation Dynamics

The BioBiped1 robot, shown in Fig. 1(c) and built within the BioBiped project, is characterized by highly compliant active and passive actuation comprised of nine mono- and biarticular human-like muscle-tendon structures.[9] These structures represent the muscle groups that are essential during human locomotion (cf. Fig. 1(a)). We differentiate between bidirectional and unidirectional electrically driven series elastic actuators, referred to as b-SEA and u-SEA, respectively.[10] As shown in Fig. 1(b), the hip joint is actuated by a b-SEA representing the antagonist-agonist muscle pair *Gluteus Maximus* (GL) - *Iliopsoas* (ILIO). The knee and ankle joints are each actuated by a combination of a u-SEA and its passive counterpart: in the knee *Vastus lateralis* (VAS) - *Popliteus* (PL) and in the ankle *Soleus* (SOL) - *Tibilias anterior* (TA). While the extensor function is actively supported, flexion in the opposing direction is invoked by a passive monoarticular structure. In addition, each leg has three passive biarticular structures, each connecting two joints and transferring power from the proximal to the distal joints: *Rectus femoris* (RF), *Biceps Femoris* (BF), and *Gastrocnemius*

Preprint of paper which appeared in the Proceedings of the
16th International Conference on Climbing and Walking Robots and the
Support Technologies for Mobile Machines

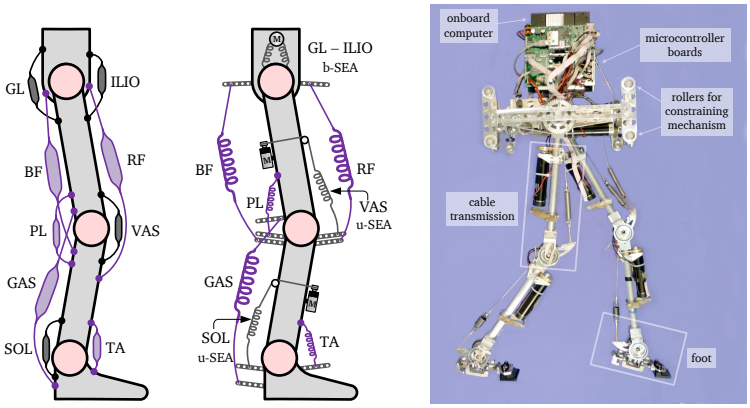

(a) (b) (c)

Figure 1. Technical realization of BioBiped1's actuation system: (a) Essential human muscle groups during locomotion, structures contributing mostly to the power generation are indicated by dark grey color; (b) technical realization of the mono- and biarticular elastic structures in the legs of BioBiped1;[10] (c) real BioBiped1 platform.

(GAS). The technical realization of all structures is described in Ref. 9. All passive structures can be attached and detached as desired.

To summarize, each joint is affected by exactly one actuated structure comprised of a DC motor and the coupled spring-tendon, but additionally also by a number of passive structures. Note that the biarticular structures affect two joints simultaneously, e.g. $\tau_{\mathrm{RF,H}}$ is the torque induced by RF on the hip joint, whereas $\tau_{\mathrm{RF,K}}$ indicates the torque caused by RF on the knee joint. For brevity, the output torque function for each joint is listed below:

$$\tau_{\mathrm{e,H}}(q_{\mathrm{H}},\theta_{\mathrm{H}},q_{\mathrm{K}}) = \tau_{\mathrm{GLILIO}}(q_{\mathrm{H}},\theta_{\mathrm{H}}) + \tau_{\mathrm{RF,H}}(q_{\mathrm{H}},q_{\mathrm{K}}) + \tau_{\mathrm{BF,H}}(q_{\mathrm{H}},q_{\mathrm{K}}) \quad (1)$$

$$\begin{aligned}\tau_{\mathrm{e,K}}(q_{\mathrm{K}},\theta_{\mathrm{K}},q_{\mathrm{A}}) = {} & \tau_{\mathrm{VAS}}(q_{\mathrm{K}},\theta_{\mathrm{K}}) + \tau_{\mathrm{PL}}(q_{\mathrm{K}}) + \tau_{\mathrm{GAS,K}}(q_{\mathrm{K}},q_{\mathrm{A}}) \\ & + \tau_{\mathrm{RF,K}}(q_{\mathrm{K}},q_{\mathrm{H}}) + \tau_{\mathrm{BF,K}}(q_{\mathrm{K}},q_{\mathrm{H}}) \quad (2)\end{aligned}$$

$$\tau_{\mathrm{e,A}}(q_{\mathrm{A}},\theta_{\mathrm{A}},q_{\mathrm{K}}) = \tau_{\mathrm{SOL}}(q_{\mathrm{A}},\theta_{\mathrm{A}}) + \tau_{\mathrm{TA}}(q_{\mathrm{A}}) + \tau_{\mathrm{GAS,A}}(q_{\mathrm{A}},q_{\mathrm{K}}) \quad (3)$$

with q_{H}, q_{K} and q_{A} denoting the hip, knee and ankle joint angle, respectively. θ_{H}, θ_{K} and θ_{A} stand for the hip, knee and ankle motor position, respectively. The single torque terms refer to the torques induced by the corresponding structure, e.g. τ_{GLILIO} is the torque exerted by the b-SEA on the hip joint. The knee joint possesses the most complex dynamics behavior, as its function includes torques applied by five out of nine structures in total. In general, the output functions are highly complex and nonlinear. Not only does each joint torque function include several torque terms, but

each torque term depends also on various parameters, such as spring stiffness, rest length and force application points to attach a tendon to the joint, where applicable. Another feature of the musculoskeletal actuation system is the high number of integrated redundant functionalities. For instance, the knee joint flexion is not only due to the passive action of PL, but might also result from the action of GAS or BF. Such redundant functionalities can be found for all joints, both for flexion and extension. This complex actuation dynamics raises the question of suitable controllers and motivates the choice of model-based trajectory planning and execution which facilitates the comparison of various leg actuation designs.

3. Method

In this section we propose a new method for model-based motion generation and control combining feedforward and feedback control for musculoskeletal robots. Based on the detailed mathematical models of the different actuator types presented in Ref. 10, we derive step-by-step the required control signals for given reference motions. An overview of the method is given in Fig. 2.

Step 1: In the first step we derive the actuated joint torques for given reference trajectories $\boldsymbol{q}_{\mathrm{d}}$. This problem is ill-posed, as the constraint forces, that are required for solving for the actuated joint torques, depend on the applied actuation torques. Therefore, a low-gain PD controller determines the required joint torques, denoted as $\hat{\boldsymbol{\tau}}_{\mathrm{e,J}}$, to move the rigid robot model along the desired motion trajectories during the forward dynamics simulations. Instead of a PD controller, it is also possible to carry out an orthogonal decomposition to project the robot dynamics onto a reduced dimensional space.[11]

Step 2: Using the numerical results obtained from the forward dynamics computation of the rigid joint-link structure, $\hat{\boldsymbol{\tau}}_{\mathrm{e,J}}$ and $\hat{\boldsymbol{q}}$, the motor angles and torques required for the elastic robot, $\boldsymbol{\theta}_{\mathrm{d}}$ and $\boldsymbol{\tau}_{\mathrm{m,d}}$, are computed analytically based on the corresponding models of the b-SEA, u-SEA and passive mono- and biarticular structure. The subscript $_d$ indicates the desired and computed variables. For brevity, only the important equations will be listed here, and not the full derivations.

The mechanical motor dynamics is composed of a frictional term, an inertial term and the torques induced by the elastic transmission on the motor, denoted as $\boldsymbol{\tau}_{\mathrm{e,M}}$:

$$\boldsymbol{\tau}_{\mathrm{m,d}} = \boldsymbol{I}_{\mathrm{m}}\,\ddot{\boldsymbol{\theta}}_{\mathrm{d}} + \boldsymbol{D}_{\mathrm{vg}}\,\dot{\boldsymbol{\theta}}_{\mathrm{d}} + \boldsymbol{\tau}_{\mathrm{e,M}} \tag{4}$$

with $\boldsymbol{D}_{\mathrm{vg}} \equiv \boldsymbol{E}(\boldsymbol{d}_{\mathrm{r}}+\boldsymbol{d}_{\mathrm{g}})$ where $\boldsymbol{E}$ is the identity matrix and $\boldsymbol{d}_{\mathrm{r}}$ and $\boldsymbol{d}_{\mathrm{g}}$ stand for the rotor and gearbox damping vectors, respectively. $\boldsymbol{I}_{\mathrm{m}}$ is the diagonal inertia matrix, computed by $\boldsymbol{I}_{\mathrm{m}} = \boldsymbol{E}\,(\boldsymbol{I}_{\mathrm{r}} + \boldsymbol{I}_{\mathrm{g}})$, where $\boldsymbol{I}_{\mathrm{r}}$ and $\boldsymbol{I}_{\mathrm{g}}$ refer to the rotor and gearbox inertia vectors, respectively.

Using $\hat{\boldsymbol{\tau}}_{\mathrm{e,J}}$ and $\hat{\boldsymbol{q}}$, we can solve Eqs. (1) - (3) for the required motor positions $\boldsymbol{\theta}_{\mathrm{d}}$. The only terms that depend on the motor position are those caused by a b-SEA or u-SEA: τ_{GLILIO}, τ_{VAS} and τ_{SOL}. In addition to the actuators, a number of passive structures contribute to the joint dynamics. Their contributions can be determined based on the simulated joint angles $\hat{\boldsymbol{q}}$. Rewriting Eqs. (1) - (3) with respect to the active terms we obtain:

$$\tau_{\mathrm{GLILIO}}(\hat{q}_{\mathrm{H}}, \theta_{\mathrm{H}}) = \hat{\tau}_{\mathrm{e,H}} - \tau_{\mathrm{RF,H}}(\hat{q}_{\mathrm{H}}, \hat{q}_{\mathrm{K}}) - \tau_{\mathrm{BF,H}}(\hat{q}_{\mathrm{H}}, \hat{q}_{\mathrm{K}}) \tag{5}$$

$$\begin{aligned}\tau_{\mathrm{VAS}}(\hat{q}_{\mathrm{K}}, \theta_{\mathrm{K}}) = {} & \hat{\tau}_{\mathrm{e,K}} - \tau_{\mathrm{PL}}(\hat{q}_{K}) - \tau_{\mathrm{RF,K}}(\hat{q}_{\mathrm{K}}, \hat{q}_{\mathrm{H}}) \\ & - \tau_{\mathrm{BF,K}}(\hat{q}_{\mathrm{K}}, \hat{q}_{\mathrm{H}}) - \tau_{\mathrm{GAS,K}}(\hat{q}_{\mathrm{K}}, \hat{q}_{\mathrm{A}})\end{aligned} \tag{6}$$

$$\tau_{\mathrm{SOL}}(\hat{q}_{\mathrm{A}}, \theta_{\mathrm{A}}) = \hat{\tau}_{\mathrm{e,A}} - \tau_{\mathrm{TA}}(\hat{q}_{\mathrm{A}}) - \tau_{\mathrm{GAS,A}}(\hat{q}_{\mathrm{A}}, \hat{q}_{\mathrm{K}}) \tag{7}$$

The right-hand sides of Eqs. (5) - (7) now contain only the known total joint torques and the torques generated by the passive, mono- and biarticular structures. The left-hand sides represent the torques excerted by the active structures and include the unknown motor positions as linear terms. The torques transmitted by these actuator types can be computed by means of the mathematical models given in Ref. 10. Combining the solutions of the left-hand sides for θ_{H}, θ_{K} and θ_{A} with the right-hand sides of Eqs. (5) - (7) yields the desired motor position trajectories. Let us exemplary formulate the equation for the hip motor position where $\tau_{\mathrm{GLILIO}} = k_{\mathrm{e}}\,(\theta_{\mathrm{H}} - \hat{q}_{\mathrm{H}})$:

$$\theta_{\mathrm{H}} = \hat{q}_{\mathrm{H}} + \frac{1}{k_{\mathrm{e}}}\,\hat{\tau}_{\mathrm{e,H}} - \frac{1}{k_{\mathrm{e}}}\,\tau_{\mathrm{RF,H}}(\hat{q}_{\mathrm{H}}, \hat{q}_{\mathrm{K}}) - \frac{1}{k_{\mathrm{e}}}\,\tau_{\mathrm{BF,H}}(\hat{q}_{\mathrm{H}}, \hat{q}_{\mathrm{K}}) \tag{8}$$

k_{e} stands for the constant torsional stiffness of the elastic spring. In order to determine the full motor torques using Eq. (4), the transmission torques induced on the motor side are needed as well. For this specific actuator, transmission torques on motor and joint side are equal, i.e. $\tau_{\mathrm{e,M\,H}} \equiv \tau_{\mathrm{GLILIO}}$ holds for variables reflected through the transmission. Due to the linearity of the transmission the solution for θ_{H} (cf. Eq. 8) is rather straightforward, in contrast to the nonlinear transmission of the u-SEA. The u-SEA of the knee, as well as of the ankle joint, has a more complex output torque function involving a cross product computation:

$$\tau_{\mathrm{VAS}}(\hat{q}_{\mathrm{K}}, \theta_{\mathrm{K}}) = \left({}^{K}\boldsymbol{p}_{\mathrm{KAJ}} \times {}^{K}\boldsymbol{F}(\hat{q}_{\mathrm{K}}, \theta_{\mathrm{K}})\right) \bullet e_Z \tag{9}$$

$$= \left({}^{K}\boldsymbol{p}_{\mathrm{KAJ}} \times \left(k_{\mathrm{e}}\,\Delta l(\hat{q}_{\mathrm{K}}, \theta_{\mathrm{K}}) \frac{{}^{K}\boldsymbol{l}(\hat{q}_{\mathrm{K}})}{\|{}^{K}\boldsymbol{l}(\hat{q}_{\mathrm{K}})\|}\right)\right) \bullet e_Z \tag{10}$$

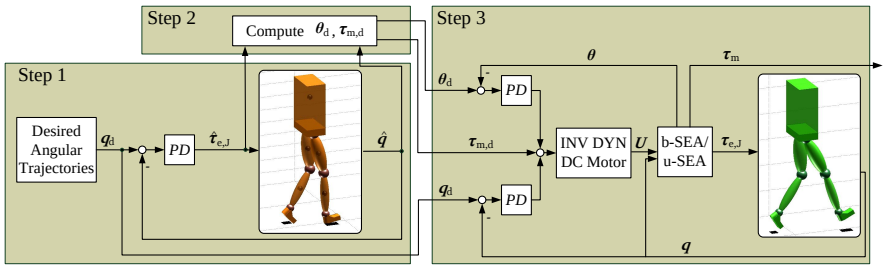

Figure 2. Controller scheme to derive the required motor control signals for given joint reference trajectories (adapted from Ref. 8).

with ${}^K\boldsymbol{p}_{\mathrm{KAJ}} \in \mathbf{R}^3$ denoting the vector to the moving tendon fixation point. ${}^K\boldsymbol{F} \in \mathbf{R}^3$ is the tendon force vector with respect to the knee coordinate system. A schematic drawing of this actuation concept as well as definitions for the spring elongation Δl and tendon length vector ${}^K\boldsymbol{l} \in \mathbf{R}^3$ are presented in Ref. 10. Note also that the transmission system exerts different torques on the motor side:

$$\tau_{\mathrm{e,MK}}(\hat{q}_{\mathrm{K}}, \theta_{\mathrm{K}}) = -r_{\mathrm{M}} \left\| {}^K\boldsymbol{F}(\hat{q}_{\mathrm{K}}, \theta_{\mathrm{K}}) \right\| \tag{11}$$

with r_{M} denoting the radius of the gearhead output shaft.

For simplicity and consistent treatment, we neglect damping terms in the computation of the inverse models. However, damping is incorporated in the dynamics equations of the motor, transmission and joint for the forwards dynamics simulation of the complete model.[10]

Step 3: In this last step, the forward dynamics of the elastic robot, i.e. the complete multibody system (MBS) dynamics model including its complex actuation, is simulated. Each actuator is PD controlled to track the computed motor positions $\boldsymbol{\theta}_{\mathrm{d}}$. The feedforward compensation term, represented by the precomputed torques $\boldsymbol{\tau}_{\mathrm{m,d}}$, constitutes the most important component of this controller (cf. Fig. 2), as it reduces the control effort. It unburdens the control loop because most of the necessary power converter excitation can be generated in the feedforward path. The PD control law is required to provide only corrections and to respond to disturbances.[12] It is also possible to choose between the two modes, either complete feedback control with high gain parameters tuned to track the reference signals very precisely or sole feedforward control exploiting the eigendynamics.

Preprint of paper which appeared in the Proceedings of the
16th International Conference on Climbing and Walking Robots and the
Support Technologies for Mobile Machines

4. Simulation Study and Results

In this section we compare the model-based approach, outlined in the previous section, with open-loop feedforward excitation of the motors. In order to realize in-place hopping motions, we first create sinusoidal patterns with the formula $y = A \sin(\omega t + \phi) + B$ based on desired leg configurations for the flexion and extension phase at the fundamental frequency $f_0 = 2\,\mathrm{Hz}$ ($\boldsymbol{q}_{\mathrm{flex}} = (q_{\mathrm{H}}, q_{\mathrm{K}}, q_{\mathrm{A}}) = (26°, -63°, 13°)$, $\boldsymbol{q}_{\mathrm{ex}} = (q_{\mathrm{H}}, q_{\mathrm{K}}, q_{\mathrm{A}}) = (13°, -26°, -13°)$). Using the motor positions required to compensate for the gravitational forces occurring during these configurations, the amplitude A, angular frequency ω, phase ϕ and offset angle B are computed to subsequently generate the motor trajectories. As, at this stage, postural stability is still neglected, the robot's upper body movements are constrained to 1D motions.[9] With the simulation parameters given in Table 1 the forward dynamics of the BioBiped1 robot model is simulated for ten cycles in MATLAB/Simulink using the ode23 (Bogacki-Shampine) solver with variable step size, relative tolerance 10^{-3} and adaptive zero-crossing options. The robot is about 1.1 m tall in extended position and weighs around 10 kg. For the segment masses and link lengths we refer to Ref. 13.

Utilizing $\hat{\boldsymbol{\tau}}_{\mathrm{e,J}}$ and $\hat{\boldsymbol{q}}$ obtained from the above simulation run, we determine the required motor positions $\boldsymbol{\theta}_{\mathrm{d}}$ and torques $\boldsymbol{\tau}_{\mathrm{m,d}}$ to apply the model-based approach and proceed as described in *Step 2* and *Step 3*. In Fig. 3 snapshots of this model-based realization of the hopping motions are illustrated. The corresponding ground reaction forces (GRF) occurring in each cycle are given below. The average duty factor and hopping height amount to 25.57 % and 0.26 m, respectively. The realized motions match very well the motions obtained by the open-loop feedforward excitation method. For the standard deviations see Table 2. Considering a motion range of about 30 ° in the hip, 40 ° in the knee and 33 ° in the ankle joint, the obtained values for σ_{q} can be regarded as insignificant. These deviations result from the deviations existing between the actual motor positions of the open-loop excitation and model-based method which are due to various reasons. Since the signals from *Step 1* are further processed to determine the motor positions and torques which include implicitly the fourfold derivation of $\hat{\boldsymbol{q}}$, it is essential to apply filtering to the signals. Filtering is also applied to the computed signals in *Step 2* to ensure that irrelevant peaks are not unnecessarily tracked by the method. This signal filtering may lead to changed configurations of $\boldsymbol{q}$ and $\boldsymbol{\theta}$ which can cause tendon slackening. Besides it should be noted, as previously mentioned, that the computation of the hip transmission torque does not consider any friction causing slight deviations, as

Table 1. Simulation parameters

Geared DC motor in hip, knee, ankle	
Motor torque constant	$k_\mathrm{t} = 2.6 \cdot 10^{(-2)}\,\mathrm{Nm/A}$
Motor rotor inertia	$I_\mathrm{r} = 3.3 \cdot 10^{(-6)}\,\mathrm{kg\,m^2}$
Motor speed constant	$k_\mathrm{v} = 2.6 \cdot 10^{(-2)}\,\mathrm{Vs/rad}$
Motor armature resistance	$R_\mathrm{a} = 0.611\,\mathrm{Ohm}$
Gearbox ratio	$n_\mathrm{g} = 66$
Gearbox inertia	$I_\mathrm{g} = 7 \cdot 10^{(-8)}\,\mathrm{kg\,m^2}$
Rotor and gearbox viscous damping	$d_\mathrm{vg} = 1.5 \cdot 10^{(-4)}\,\mathrm{Nms/rad}$
Contact model parameters[14]	
Vertical collision force constant	$k_\mathrm{c} = 8 \cdot 10^3\,\mathrm{N/m}$
Collision damping coefficient	$\lambda_\mathrm{c} = 10^4\,\mathrm{Ns/m^2}$
Sliding friction coefficient	$\mu_\mathrm{fk} = 0.6$
Sliding friction to stiction transition velocity limit	$v_\mathrm{stic} = 0.001\,\mathrm{m/s}$
Maximum stiction force coefficient	$\mu_\mathrm{fs} = 0.8$
Horizontal ground interaction stiffness	$k_\mathrm{fs} = 10^4\,\mathrm{N/m}$
Stiction damper	$d_\mathrm{fs} = 40\,\mathrm{Ns/m}$

Elastic transmissions			
Structure	**Stiffness** [N/mm]	**Attachment** [number]	**Rest angle** [deg]
VAS	15.5	4	-70
PL	6.7	1	-70
SOL	13.3	4	15
TA	4.1	1	15

Motor controller gains	
P-gain hip b-SEA $k_\mathrm{p,H} = 200$	D-gain hip b-SEA $k_\mathrm{d,H} = 50$
P-gain knee VAS $k_\mathrm{p,K} = 30$	D-gain knee VAS $k_\mathrm{d,K} = 8$
P-gain ankle SOL $k_\mathrm{p,A} = 30$	D-gain ankle SOL $k_\mathrm{d,A} = 4$

friction is included in the forward model. Hence, it is even more noteworthy that the model-based approach is capable of tracking the original motions incorporating dynamic ground contacts so well, without any ground contact sensing. The most important result is that the motions can be tracked without increasing the power consumption (see the values for σ_u and σ_i). Also, it should be mentioned that the actually generated motor torques $\boldsymbol{\tau}_\mathrm{m}$ agree very well with the computed feedforward torques $\boldsymbol{\tau}_\mathrm{m,d}$. This feedforward compensation term can highly reduce the efforts of the feedback control and in this way turn the motion control more robust in the presence of external disturbances.

Table 2. Standard deviations of the model-based generated from the open-loop excitation trajectories.

Joint	**Hip**	**Knee**	**Ankle**
$\sigma_\mathrm{q}[^\circ]$	0.8252	1.7741	3.0559
$\sigma_\theta[^\circ]$	0.2789	4.2434	3.2883
σ_u[V]	0.22277	3.1192	1.7518
σ_i[A]	0.3485	0.8337	0.5538

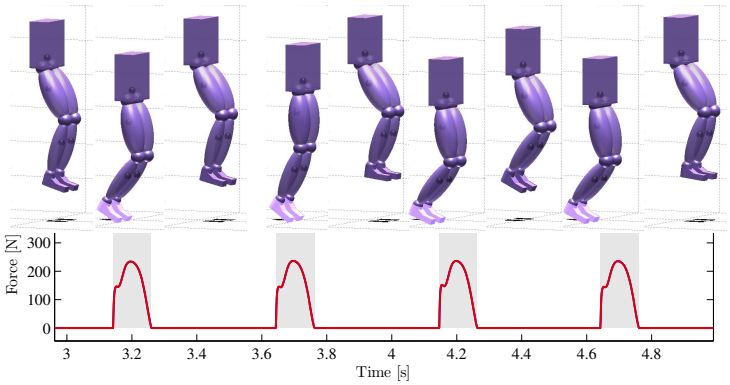

Figure 3. Snapshots of the simulated BioBiped1 robot tracking the in-place hopping motions obtained from the open-loop excitation of the motors based on the model-based approach. In the lower diagram the corresponding patterns of the GRF of both legs, which overlap due to the symmetric movements, are depicted.

5. Conclusions

In this paper we presented a model-based elastic tendon controller for musculoskeletal robots using as reference motions joint angle trajectories. The standard deviations showed that the method performs as well as open-loop feedforward oscillatory excitation providing additionally a number of benefits.

By this method, the complete musculoskeletal system including all tendon structures and the corresponding dimension space can be studied. For instance, it is possible to vary the spring stiffness or the attachment points for a defined leg actuation design and recompute the changed actuation requirements demanded of the motors. Being well suited for systems with highly redundant actuation, the method allows to precompute each structure's contribution to the overall joint dynamics and to adapt the requirements demanded of the motors to achieve, for example, energy-efficient locomotion. It can be analyzed how varied actuation requirements for the same reference motions result in different locomotion performance characterized by selected criteria such as the duty factor, energy consumption or hopping height. In this context, the method has clear advantages over basic sinusoidal motor excitations. Such concept is tremendously important to advance musculoskeletal designs and their use.

An important application of this method is also the dimensioning of the motor-gearboxes prior to a robot's construction.[8] Future work includes the implementation of the method on the hardware platform. Further, op-

timization of selected performance criteria will be conducted incorporating the outcomes of the approach as initial trajectories. In this context, it is also interesting to exploit the benefits of machine learning methods.[15]

Acknowledgements

This work was supported by the German Research Foundation (DFG) under grant no. STR 533/7-1. Special thanks go to Thomas Lens for helpful discussions. The BioBiped1 robot was developed within the BioBiped project.

Bibliography

1. K. Hosoda *et al.*, "Pneumatic-driven jumping robot with anthropomorphic muscular skeleton structure," *Autonomous Robots*, vol. 28, no. 3, pp. 307–316, 2010.
2. T. J. Klein, T. Phuam, and M. A. Lewis, "On the design of walking machines using biarticular actuators," in *CLAWAR*, 2008.
3. R. Niiyama, "Design of a musculoskeletal Athlete robot: A biomechanical approach," in *CLAWAR*, 2009, pp. 173–180.
4. Y. Asano *et al.*, "Lower thigh design of detailed musculoskeletal humanoid "Kenshiro"," in *IROS*, 2012, pp. 4367–4372.
5. K. Hosoda *et al.*, "Biped robot design powered by antagonistic pneumatic actuators for multi-modal locomotion," *Robotics and Autonomous Systems*, vol. 56, pp. 46–53, 2007.
6. F. Iida, J. Rummel, and A. Seyfarth, "Bipedal walking and running with compliant legs," in *ICRA*, 2007, pp. 3970–3975.
7. A. D. Luca, "Feedforward/feedback laws for the control of flexible robots," in *ICRA*, 2000, pp. 233 –239.
8. K. Radkhah and O. von Stryk, "Actuation requirements for hopping and running of the musculoskeletal robot BioBiped1," in *IROS*, 2011, pp. 4811–4818.
9. K. Radkhah *et al.*, "Concept and design of the BioBiped1 robot for human-like walking and running," *IJHR*, vol. 8, no. 3, pp. 439–458, 2011.
10. K. Radkhah, T. Lens, and O. von Stryk, "Detailed dynamics modeling of BioBiped's monoarticular and biarticular tendon-driven actuation system," in *IROS*, 2012, pp. 4243 – 4250.
11. M. Mistry, J. Buchli, and S. Schaal, "Inverse dynamics control of floating base systems using orthogonal decomposition," in *ICRA*, 2010, pp. 3406–3410.
12. G. Ellis, *Control System Design Guide*. Elsevier Academic Press, 2004.
13. K. Radkhah and O. von Stryk, "Exploring the Lombard paradox in a bipedal musculoskeletal robot," in *CLAWAR*, 2013.
14. T. Lens, K. Radkhah, and O. von Stryk, "Simulation of dynamics and realistic contact forces for manipulators and legged robots with high joint elasticity," in *ICAR*, 2011, pp. 34–41.
15. D. Mitrovic, S. Klanke, and S. Vijayakumar, "Adaptive optimal feedback control with learned internal dynamics models," in *From Motor Learning to Interaction Learning in Robots*, Springer, 2010, vol. 264, pp. 65–84.